Journal of Colloid and Interface Science **245,** 178–186 (2002)
doi:10.1006/jcis.2001.7938, available online at http://www.idealibrary.com on IDEAL®

Batch Gravitational Sedimentation of Slurries

C. P. Chu,* S. P. Ju,* D. J. Lee,*,[1] and K. K. Mohanty†

*Chemical Engineering Department, National Taiwan University, Taipei, Taiwan, 10617; and †Chemical Engineering Department, University of Houston, Houston, Texas 77204-4792

Received October 25, 2000; accepted August 30, 2001

We investigated the batch settling behavior of the kaolin slurry and the UK ball clay slurry at various initial solids fractions (ϕ_0s) using a computerized axial tomography scanner (CATSCAN). The spatio-temporal evolutions of solids fractions in the consolidating sediments were continuously monitored. Since the interface between the sediment and the supernatant of the investigated slurries was blurred, an averaging procedure was employed to estimate their null-stress solids fractions (ϕ_gs). Besides the rather slow settling for the high-ϕ_0 slurries, the basic settling characteristics resemble each other regardless of whether $\phi_0 > \phi_g$ or vice versa. The above-mentioned experimental data reveal that the investigated slurries are neither purely elastic nor purely plastic in rheological behavior. On contrary to most model works a blurred supernatant-sediment interface makes difficulty in the gel point determination. During initial settling the high-ϕ_0 slurries clearly exhibit a finite yield stress to resist deformation. That is, the slurries are plastic fluids. However, the network structure in the slurries deteriorates gradually in the subsequent settling stage while the final, equilibrated sediment reveals a continuous distribution in solids fraction. Restated, the final sediment possesses as a purely elastic characteristic. The model parameters of theory by Buscall and White were regressed by the dynamic consolidating sediment data, while those by Tiller and Leu were obtained using the final equilibrated sediment data. Calculations from both models reveal that ball clay slurry is more compressible than is the kaolin slurry. The high-ϕ_{S0} slurry would yield the less compressible sediment. © 2002 Elsevier Science

Key Words: **CATSCAN; sedimentation; solids fractions; yield stress.**

INTRODUCTION

Sedimentation characteristics of slurries are important in settler/thickener design and operation. Theorists like Coe and Clevenger (1), Kynch (2), and Talmadge and Fitch (3) ignored the role of the rising sediment. Tiller (4) refined the Kynch theory to consider the effect of increasing sediment during sedimentation. Fitch (5) further investigated this theory and modified the procedures to determine the characteristic lines. Font (6, 7) reviewed these works and discussed the compression zone effects in batch sedimentation.

The way the solids fraction (volume fraction of solid phase, ϕ) changes with solid pressure (P_S) governs the rheological characteristics of the consolidating sediment. As Koenders and Wakeman (9) revealed, most related works assumed an elastic filter cake having the following power-law type constitutive equation:

$$\phi = \phi_g \left(a + \frac{P_S}{P_0} \right)^{\beta}, \qquad [1]$$

where a can be 0 or 1. ϕ_g is the null-stress solids fraction or the gel point if $a = 1$ (9). P_0 represents the characteristic solid pressure (10). Equation [1] assumes that ϕ depends sorely on the local solid pressure P_S. Lee and Wang (11) summarized the literature works adopted constitutive equations following Eq. [1]. Kos (12) further assumed that the solids fraction should depend not only on the local solid pressure, but also on its gradient. Shirato *et al.* (13) refined Eq. [1] for describing the time-dependent response of filter cake using a linear visco-elastic model. Tien *et al.* (14) modified Eq. [1] to incorporate the fine migration effects.

Buscall and White (15) and Ayzerais *et al.* (16) proposed a consolidation model considering the flocculated slurry as a purely plastic body that possesses a yield stress ($P_y(\phi)$). If the local pressure of sediment exceeds P_y, the network structure would yield. Buscall and White (15) proposed the following constitutive equation:

$$\frac{D\phi}{Dt} = k(\phi, P)[P - P_y(\phi)], \quad P > P_y(\phi) \qquad [2a]$$

$$\frac{D\phi}{Dt} = 0, \quad P \le P_y(\phi), \qquad [2b]$$

where $D(\ )/Dt$ denotes the material derivative and k is the "dynamic compressibility" of the suspension (9). This model had been extensively applied to sedimentation processes of flocculated suspensions (see, for instance, (17–21)).

The governing equations controlling the liquid flows in the suspension or in the sediment are different (4). The null-stress solids fraction (ϕ_g) represents the threshold value above which the particles in a suspension physically contact each other and form a continuous phase through which the solid pressure could be directly transmitted. Tiller and Khatib (22) proposed two extrapolating procedures for estimating ϕ_g values. Lu *et al.* (23)

[1] To whom correspondence should be addressed. Fax: +886-2-2362-3040. E-mail: djlee@ccms.ntu.edu.tw.

0021-9797/02 $35.00

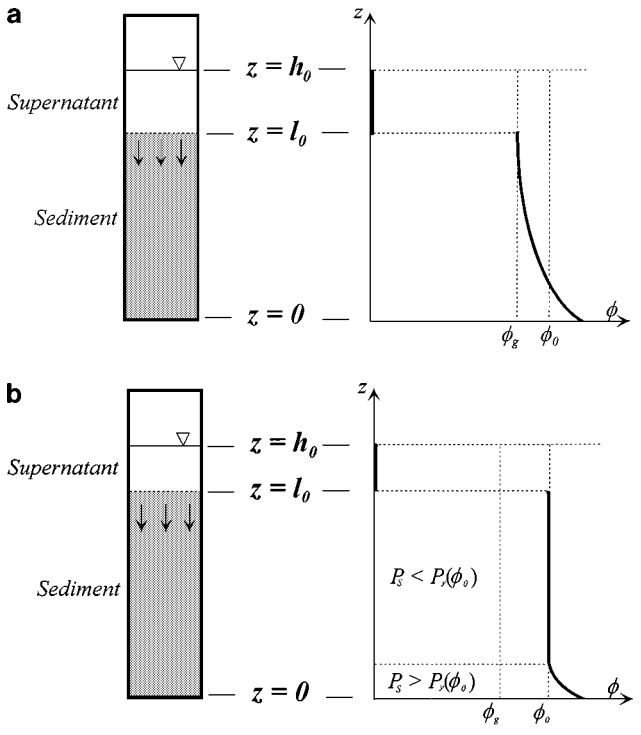

FIG. 1. Schematics of slurry settling. (a) Purely elastic sediment; (b) purely plastic sediment.

adopted low-head filtration test to determine the surface cake porosity and examine the effects of slurry concentration and operating conditions. Determination of ϕ_0 for certain slurries is extremely difficult since the interface between the sediment and the suspension could be blurred. The sudden jump in solids fraction when moving from settling slurry to sediment as suggested by the idealized theory may not be easily observed (as discussed later).

Researchers adopted nondestructive techniques to obtain the relevant variable in the solid/liquid separation processes as a function of space and time, such as the use of γ-ray (18, 24), NMR (25–27), and X-ray (17, 28–33). Buscall (34) reviewed the pertinent literature before 1990. Shen *et al.* (19) adopted the yield-stress model by Buscall and White (15) for interpreting their settling data, and noted that the model was valid during the initial phase of settling/filtration of the "pliant" systems (with initial solid weight exceeds the corresponding yield stress). For the "stiff" systems (with initial solid weight being lower than the yield stress), on the other hand, no consolidation occurred in the initial stage of experiments.

We consider the cases at $\phi_0 > \phi_g$ with all particles in the initial suspension physically contact with each other and form a network matrix. Figure 1a represents the one-dimensional sedimentation process with the purely elastic sediment, in which $z = 0$ denotes the bottom and $z = h_0$ represents the slurry surface. Since the transmission of solid pressure through the network the sediment would continuously yield at the beginning of the test. Restated, no portion of the sediment could be kept at ϕ_0 while no constant-ϕ_0 regime could be noticeable in the sediment. Moreover, the solids fraction in the final sediment should be of a continuously varying manner with no apparent constant-ϕ_0 regime (like Fig. 1a). For a purely plastic sediment with a finite yield stress, on the other hand, even at $\phi_0 > \phi_g$ the sediment would not deform if the local solid pressure has not exceeded $P_y(\phi_0)$. Therefore, a constant-ϕ_0 regime could persist during settling (Fig. 1b). The final, equilibrated sediment would also possess the constant-ϕ_0 regime (like Fig. 1b). The batch sedimentation tests of high-ϕ_0 slurries could therefore provide the information on the validity of the above-mentioned model frameworks.

This work employed the computerized axial tomography scanner (CATSCAN) for investigating the batch-settling behavior of kaolin slurry and UK ball clay slurry, particularly on the effects of ϕ_0. We first demonstrated that, since the two investigated slurries exhibit a blurred supernatant–sediment interface due to marked back-diffusion effect, the determination of their ϕ_g values were made through an averaging procedure. Then, we revealed the feasibility of using the purely elastic or the purely plastic constitutive models to interpret the obtained sedimentation data.

EXPERIMENTAL

Samples

Kaolin slurries and UK ball clay slurries were prepared by mixing fixed amount of powders with 0.1 M $NaClO_4$ solution in distilled water to provide a high ionic strength to prevent the interference of other ions that might be released from the particle surfaces. The pH values were fixed at 7.0. The particle size distribution of slurry was determined by a Sedigraph

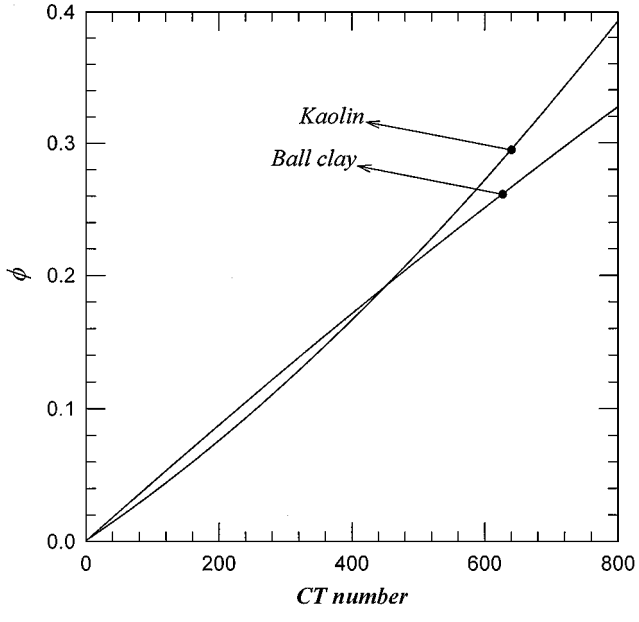

FIG. 2. The relationship between CT number and solids fraction in kaolin and clay slurries.

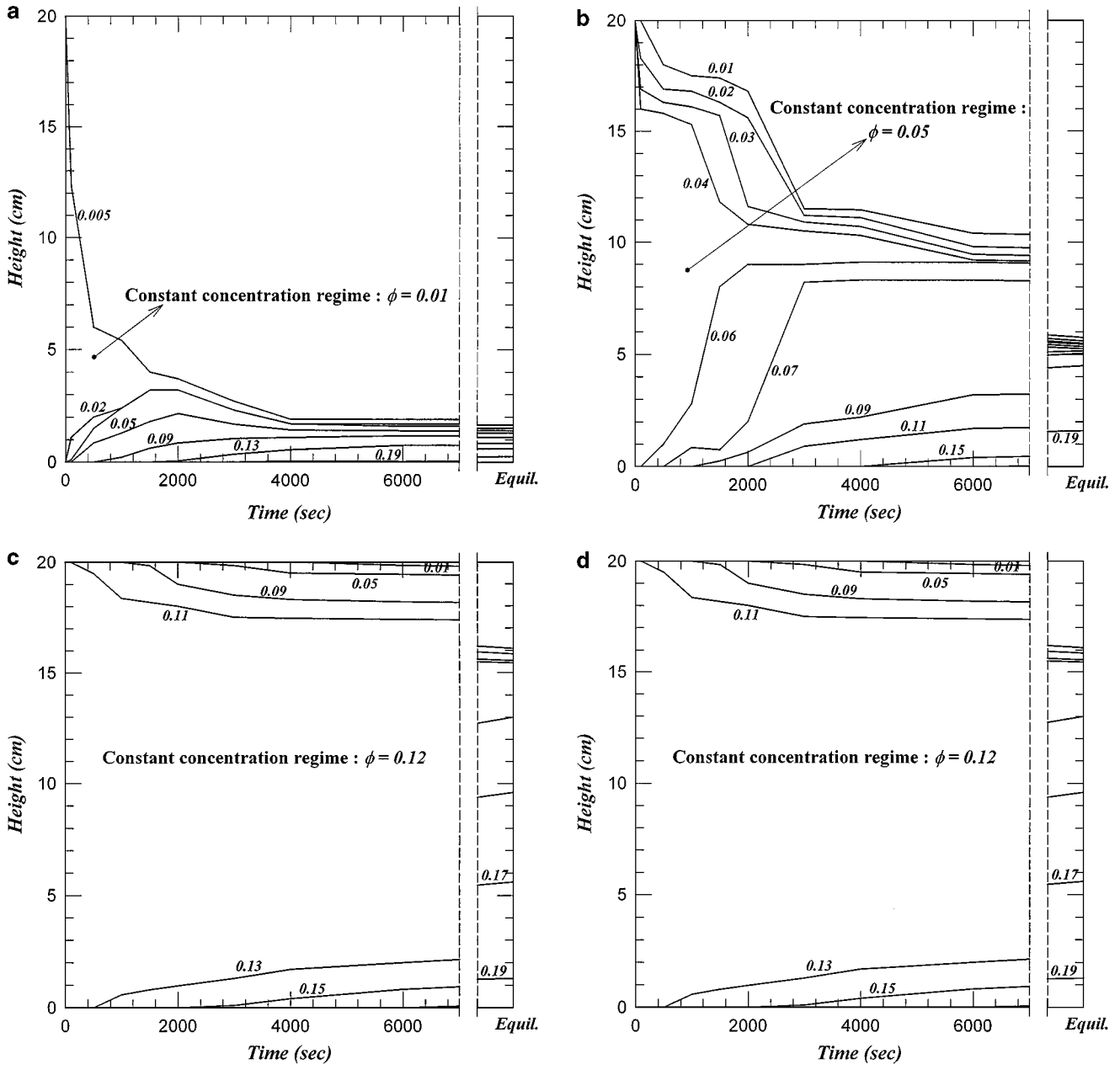

FIG. 3. The time evolutions of solids fraction for kaolin slurries. (a) $\phi_0 = 0.01$; (b) $\phi_0 = 0.05$; (c) $\phi_0 = 0.08$; (d) $\phi_0 = 0.12$; (e) $\phi_0 = 0.15$.

5100 C (Micromeritics), giving a mean diameter of 6.3 μm for kaolin slurry and 2.5 μm for clay slurry. An Accupyc Pycometer 1330 (Micromeritics) measured the true solid density. The results are 2730 kg/m^3 for kaolin powders and 2580 kg/m^3 for ball clay powders. The Zetasizer 2000 (MARLVERN) measured the ζ-potentials of suspension. The results are -17.7 mV for kaolin slurry and -22.1 mV for clay slurry.

CATSCAN

Batch settling experiments were conducted in a settling cylinder that had a height of 20 cm and a diameter of 9.5 cm, and were continuously monitored with the CATSCAN (DeltaScan 2060; 100 kV, 75 mA). The X-ray attenuations, which are normally presented as dimensionless scale, the CT number (35), could be obtained from a horizontal section. Bergstrom (18) adopted similar procedures using their γ-ray apparatus. Preliminary tests revealed that the CT number for the 0.1 M $NaClO_4$ solution is essentially zero since the dissolved salts do not absorb a significant amount of X-ray. Furthermore, the correlations between CT number and the solids fraction are noted for the kaolin and clay slurries, as demonstrated in Fig. 2. The uncertainties in axial position measurement and the local solid volume fraction

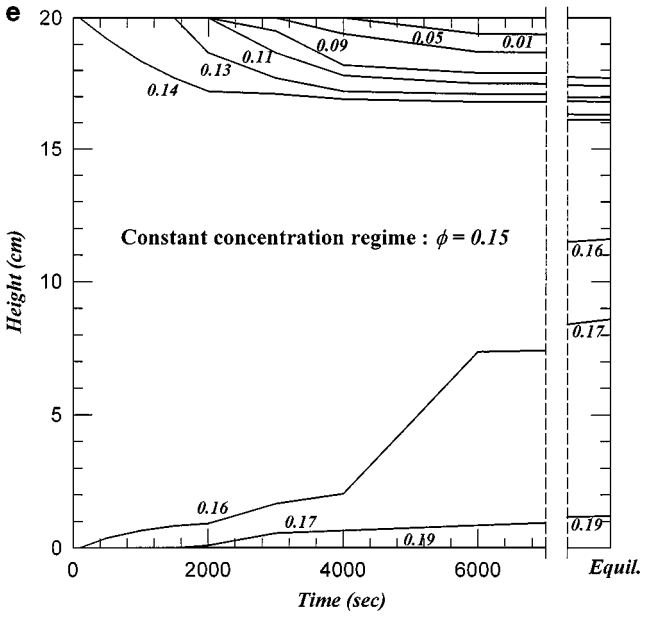

FIG. 3—*Continued*

were 2.5 mm and 0.1%, respectively, which are close to those reported in Auzerais *et al.* (17).

TIME EVOLUTIONS

Figures 3 and 4 depict the spatio-temporal evolutions of cross-sectional average solids fraction measured for kaolin and clay slurries during the first 6000 s and those at equilibrium. The mean solids fraction is interpreted as follows:

$$\phi_{\text{mea}} = \frac{\int_0^{h_0} \phi \, \mathrm{dz}}{h_0}, \qquad [3]$$

where h_0 is 20 cm, the height of the slurry. The calculated ϕ_{mea} data all range from 0.98 to $1.03\phi_0$, which partially support the accuracy of the solids fraction distributions presented in Figs. 3 and 4.

For both slurries, the settling rates decrease substantially with increasing ϕ_0, while the effects are more significant for the clay slurries than for the kaolin slurries. For all slurries initially at ϕ_0, a sediment layer appears at the tube bottom during settling, while a constant-concentration regime at ϕ_0 retains above this layer regardless of the range of ϕ_0. The basic characteristics of settling are similar for slurries at $\phi_0 > \phi_g$ to those at $\phi_0 < \phi_g$.

Figures 5a and 5b depict the solids fraction distributions in the final, equilibrated sediment. The clay slurry at $\phi_0 = 0.15$ exhibits a very blurred region above the observed sediment and is excluded in Fig. 5b. For most slurries examined herein, the interface between the sediment and the supernatant (if any) is blurred. No apparent jump in solids fraction over the so-called "supernatant-sediment" interface is noted on all curves. Previous studies could neither illustrate such a jump (9, 17, 32, 33, 36). Since the X-ray beam is of a finite thickness, the length of the transition zone should be less than the resolution provided by the present CT scanner if a distinct interface does exist. Also the Brownian motion of colloidal particles may provide a "diffusion" effect on the settling sediment (37). The CATSCAN profiles could not directly measure the ϕ_g values for the present slurries. Before the position of the interface can be determined, no reliable theoretical analyses could be made.

As Fig. 5 reveals, an "interfacial zone" of width approximately 1 cm exists in all equilibrated solids' fraction curves, which bridges the supernatant regime and the sediment regime. Although one could not distinctly identify the ϕ_g values from Fig. 5, it is clear from these curves that the portion of slurry exhibiting a solids fraction exceeding 0.10 should be definitely regarded as the sediment. A procedure is adopted herein to estimate the ϕ_g values. Since the present ultimate error for solids fraction estimation is 0.1%, the position where $\phi = 0.1\%$ is taken as the upper surface of the equilibrium sediment. The "interfacial zone" between the suspension and the sediment is taken from the surface ($\phi = 0.1\%$) to 1 cm below. The average solids fraction over this 1-cm zone is defined as ϕ_g. The corresponding vertical distance from bottom to the point at which $\phi = \phi_g$ is termed as l_0 (sediment height). The average solids fraction in the sediment ϕ_{av} is defined as

$$\phi_{\text{av}} = \frac{\int_0^{l_0} \phi \, \mathrm{dz}}{l_0}, \qquad [4]$$

The estimated null-stress solid fractions are presented as circles in Figs. 5a and 5b and are illustrated together with the ϕ_{av}s in Figs. 6a and 6b. Tiller and Khatib (22) proposed that as ϕ_0 increases the ϕ_g would first decrease, after passing a minimum point (approximately at $\phi = 0.1$), and then increase with increasing ϕ_0 up to 0.5. Apparently the values depicted in Figs. 6a and 6b do not change much with ϕ_0. Hypothesis tests reveal that there exists no apparent correlation between the ϕ_g values and the ϕ_0 data at a confidence interval of 95%.

The dashed lines in Figs. 6a and 6b represent the 45° lines at $\phi_0 = \phi_g$, which intercept the estimated ϕ_g at 0.074 and 0.082 for kaolin and clay slurries, respectively. Restated, although the procedures to determine ϕ_0 deem arbitrary, a threshold solids fraction of $\phi_g \approx 0.08$ could be used to distinguish slurry from its sediment. This value correlates with the results of Buscall and White (15) that the ϕ_0 ranges 0.05 to 0.3 for particulate suspensions. At $\phi_0 > 0.08$, the particles in the present slurries would physically contact each other and the whole slurry should be regarded as the sediment body at the start of the test.

The experimental range (0.01–0.15) has covered both the $\phi_0 < \phi_g$ and the $\phi_0 > \phi_g$ cases. Hence, the existence of the constant-ϕ_0 regime in Figs. 3 and 4 represents the yield stress

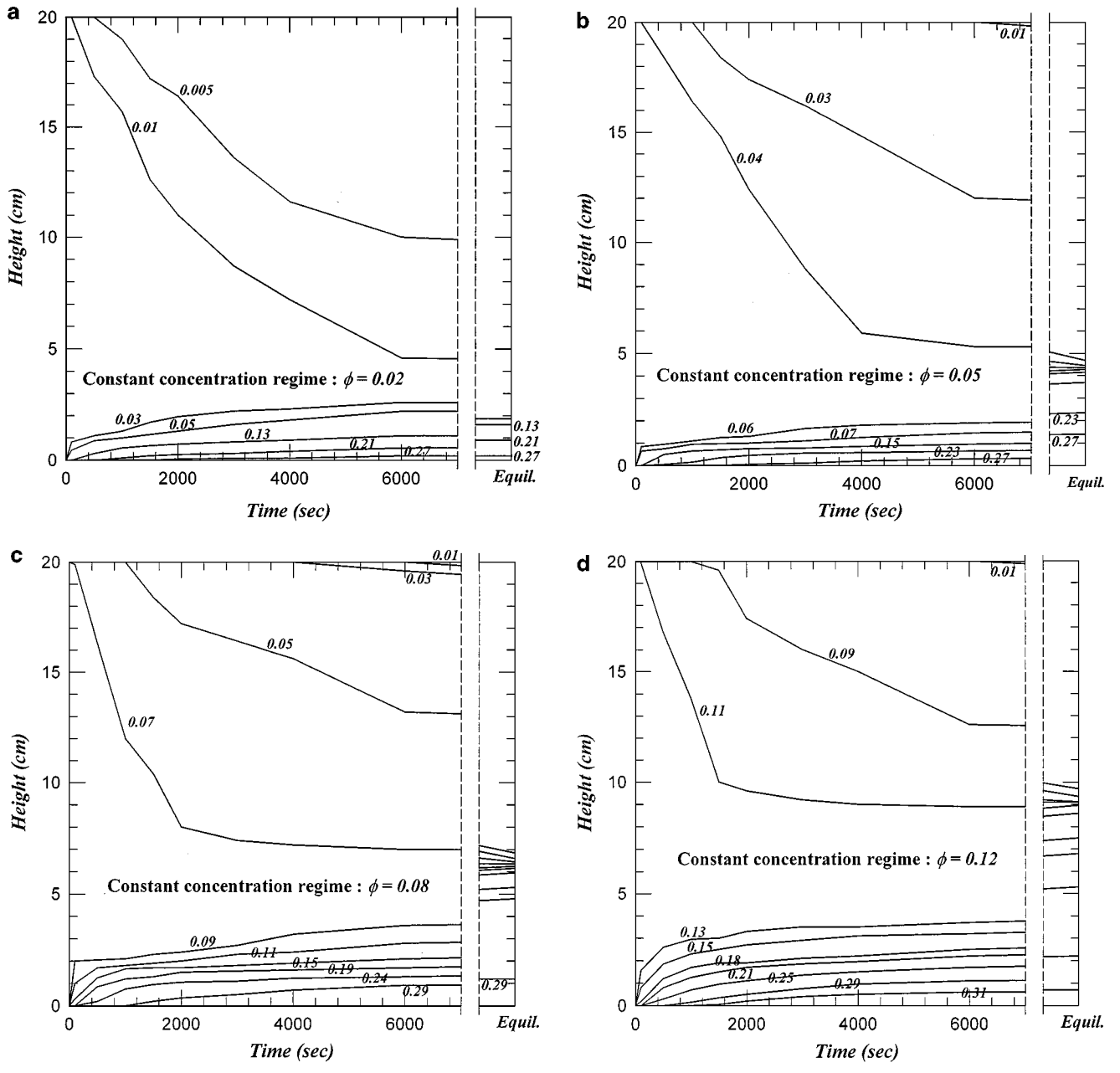

FIG. 4. The time evolutions of solids fraction for clay slurries. (a) $\phi_0 = 0.02$; (b) $\phi_0 = 0.05$; (c) $\phi_0 = 0.08$; (d) $\phi_0 = 0.12$; (e) $\phi_0 = 0.15$.

of the settling sediment, thereby supporting the purely plastic model by Buscall and White (15). As settling proceeds, the constant-ϕ_0 regime in Figs. 3 and 4 gradually shrinks, accompanied by the expansion of the supernatant and sediment zones. Equilibrium could be reached at settling time ranging from 48 h to 1 week, depending on the slurry species and the ϕ_0. It is noticeable that the final sediment exhibits no constant-ϕ_0 regime. This observation, on the other hand, favors the purely elastic model by Tiller and Leu (10). Shen *et al.* (19) also questioned the existence of the yield stress. Apparently neither the purely elastic nor the purely plastic constitutive equations could satisfactorily interpret the whole range of sedimentation process. At the start of the high-ϕ_0 tests a network of finite yield stress apparently exists. However, this structure seems degraded continuously at the bottom of the constant-ϕ_0 regime, evidenced by the increasing L_c values in Figs. 3 and 4.

FINAL SEDIMENT

As Fig. 3 demonstrates, the equilibrated solids fractions for kaolin slurries at bottom are all around 0.2 regardless of their ϕ_0 values, indicating that the kaolin slurry is not very compressible

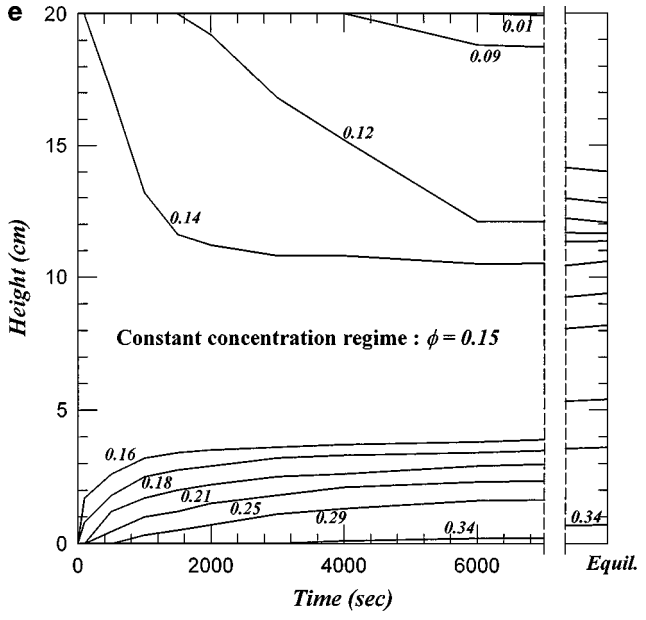

FIG. 4—*Continued*

to the applied compressive pressure. On the other hand, clay slurries could be compacted more readily to form the sediment of higher solids fraction when ϕ_0 increases (for instance, as depicted in Figs. 4a–4e, at 6000 s $\phi = 0.28$ and 0.34 for $\phi_0 = 0.02$ and 0.15, respectively). Restated, the clay sediment is more compressible than is the kaolin sediment.

Quantitative evaluation of sediment compressibility requires the local solid pressure data for the slurries. At equilibrium, the solid pressure gradient could be stated as follows:

$$\frac{\partial P_S}{\partial t} = -\Delta\rho g\phi, \qquad [5]$$

where $\Delta\rho$ is the density difference between the solid and liquid. Hence, the local solid pressure at height z is expressed as follows:

$$P_S = \Delta\rho g \int_0^z \phi \, dz. \qquad [6]$$

The solid pressure at bottom ($P_S|_{z=0}$) could be estimated based on the solids fraction data in Fig. 5 and Eq. [6] with $z = 0$. Figures 6a and 6b also represent the estimated $P_S|_{z=0}$ data as functions of ϕ_0. All $P_S|_{z=0}$ data at equilibrium are proportional to ϕ_0, or are equal to the buoyant weight of the solid particles. This also confirms the accuracy of the present experimental measurement.

Local solid pressure data could be evaluated based on Eq. [6]. Figures 7a and 7b illustrate the ϕ versus P_S curves in the final sediment. Despite certain data scattering, the local solids fraction decreases continuously with increasing ϕ_0 at some fixed effective pressure. Comparisons between clay and kaolin slurries reveal that the former exhibits a more compressible structure than is the latter.

The local structure in the sediment would be degraded owing to gravity consolidation to a level counterbalancing the corresponding yield stress. Therefore, the $\phi - P_S$ curves in Fig. 7 represent the $\phi - P_y(\phi)$ correlations. As Fig. 7 reveals, the sediment yields more readily at the low solids fraction regime than the high regime. The sediment was consolidated from the gel point to around 12–15% at a pressure less than 1–2 Pa. At a higher pressure, the sediment yields more slowly with the applied pressure. For instance, for kaolin slurry at $\phi_0 = 15\%$ the solids fraction increases from 15 to 20% over a pressure up to

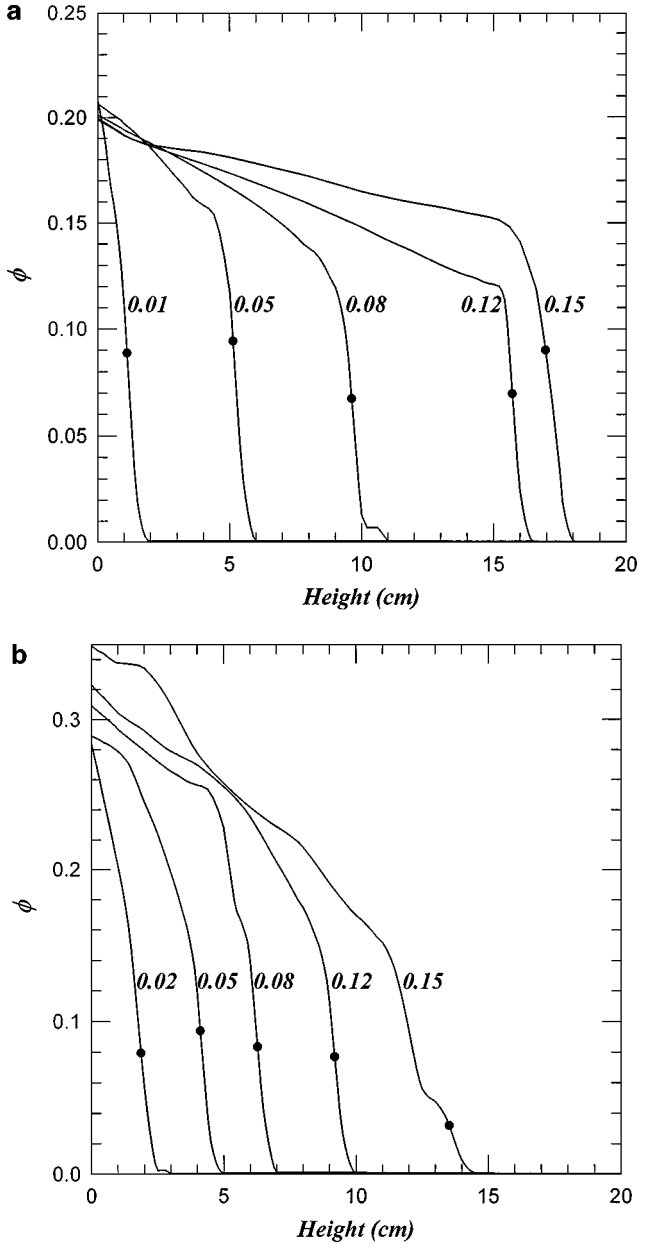

FIG. 5. The solids fraction distributions in equilibrated sediments. (a) Kaolin slurry, and (b) clay slurry. Black circles denote the corresponding null-stress solid fractions.

400 Pa. In fact, the structure of the final sediment at high ϕ_0 would depend only weakly on the applied pressure.

Empirical equations could correlate the $\phi - P_S$ curves in Fig. 7. Here we employ Eq. [1] in sample calculations since the fitting could be achieved using graphical method proposed by (10). The obtained parameters according to the graphical method were adopted as the initial guess to nonlinear regression of Eq. [1] with the experimental data. Table 1 lists the obtained results. The parameter P_0 is rather low, generally around or less than 1 Pa, indicating that these slurries would largely deform at the low-pressure regime. Also, the β values are lesser for clay slurries than those for the kaolin slurries, stating that the former is more compressible than the latter. Finally, the higher ϕ_0 would yield the lower P_0 and β. Restated, the slurry with a high initial solid concentration would deform quickly at the low solid pressure, but would resist more readily the external applied pressure at a greater solid pressure. Therefore, in the practical regime the high-ϕ_0 systems would pack more readily when initially form, but become rather "stiff" owing to the associated large yield stress.

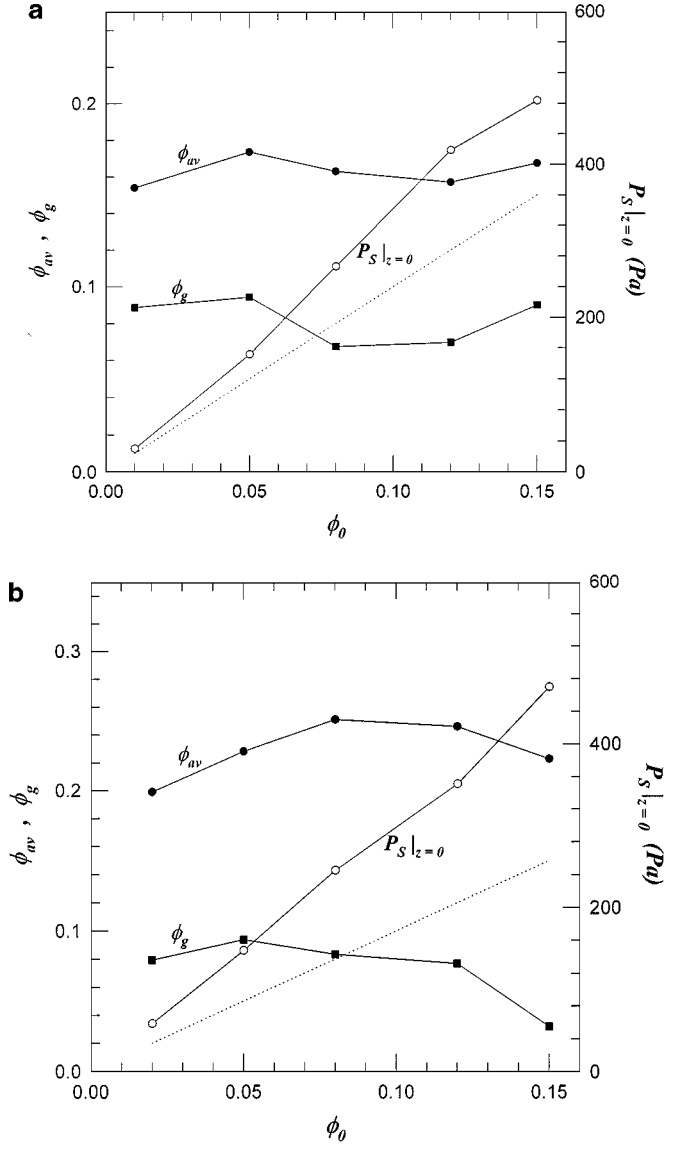

FIG. 6. The null-stress solids fraction ϕ_g, average solids fraction ϕ_{av} in sediment, and solid pressure at bottom $P_S|_{z=0}$ at different ϕ_0; (a) kaolin slurry and (b) clay slurry.

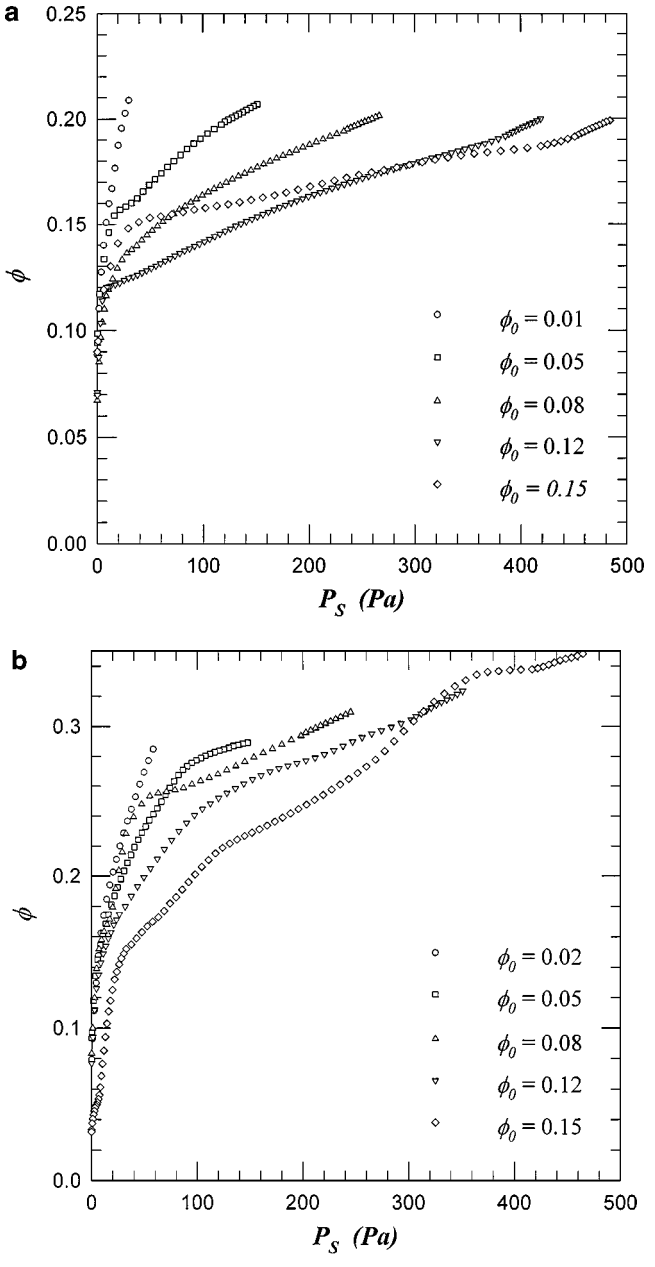

FIG. 7. The solids fraction distributions in sediment versus solid pressure at different ϕ_0: (a) kaolin slurry, and (b) clay slurry.

CONSOLIDATING SEDIMENT

For demonstrating the sediment compaction effects, only the portion of sediment with $\phi > \phi_g$ would be herein considered.

TABLE 1
Model Parameters Obtained in This Work

ϕ_0	ϕ_g	$U_0K(\phi_0)$ (m/s)	P_v (Pa)	P_0 (Pa)	β
		Kaolin slurries			
0.01	0.089	NA	NA	1.60	0.30
0.05	0.094	NA	NA	0.80	0.15
0.08	0.067	8.49×10^{-5}	207	0.50	0.18
0.12	0.070	6.77×10^{-5}	377	0.50	0.15
0.15	0.100	6.13×10^{-5}	448	0.90	0.10
		UK ball clay slurries			
0.02	0.079	NA	NA	1.20	0.35
0.05	0.094	NA	NA	1.05	0.25
0.08	0.083	1.36×10^{-4}	96	0.40	0.20
0.12	0.077	1.11×10^{-4}	324	0.65	0.23
0.15	0.082	1.01×10^{-4}	432	0.37	0.70

The solid velocity of sediment at ϕ_0 by Landman and Russel (38) is stated as follows:

$$u_S(\phi_0) = -\frac{dy}{dt} = -U_0K(\phi_0)\left(1 - \frac{\partial P_S/\partial z}{\Delta\rho g\phi_0}\right)$$
$$= -U_0K(\phi_0)\left[1 - \frac{P_y(\phi_0)}{\Delta\rho g\phi_0(y - L_c)}\right], \quad [7]$$

where U_0 is the terminal velocity of individual particle; K is the hindered factor; $\Delta\rho$, the density difference between the solids and the liquid; g, the gravitational acceleration; y, the upper interfacial height where $\phi = \phi_0$; and L_c, the height where ϕ deviates from ϕ_0 (19). Equation [5] is valid for the consolidating sediment with $\phi > \phi_0$. A regime of constant ϕ_0 is assumed to exist in the consolidating sediment over the range of $z = y$, where $P_S = 0$ to $z = L_c$, where $P_S = P_y(\phi_0)$. Hence, the plot with dy/dt versus $1/(y - L_c)$ estimates the U_0K and P_y at $\phi = \phi_0$ with linear regression analysis.

The investigated slurries possess a blurred suspension, while the solid pressure accumulated at y_g, where $\phi = \phi_g$. Therefore, Eq. [5] needs correction as follows:

$$\frac{dy}{dt} = U_0K(\phi_0)\left[1 - \frac{P_y(\phi_0) - P_g}{\Delta\rho g\phi_0(y - L_c)}\right], \quad [8]$$

where P_g is the accumulated solid pressure at y and could be approximated as

$$P_g = P_S|_{z=y} \approx \Delta\rho g \int_{y_g}^{y} \phi \, dz. \quad [9]$$

If Eq. [8] were valid for describing the dynamics of the consolidating sediment, the curves for dy/dt versus $1/(y - L_c)$ data should reveal a linear character. Figure 8 shows some dy/dt versus $1/(y - L_c)$ data sets of $\phi_0 > \phi_g$ tests. Apparently the curves in Fig. 8 reveal a linear relation during early stage of settling. For instance, for kaolin slurry at $\phi_0 = 8\%$, Eq. [1] could describe the consolidation at testing time less than 1000 s. After the initial stage the settling becomes very slow (very small dy/dt) while the linear relationship breaks down. This observation corresponds to the observation by Shen *et al.* (1994). The yield stress of the investigated slurries could not sustain the integrity of the constant-ϕ_0 regime which deteriorates continuously with time.

Table 1 lists the best-fit $P_y(\phi_0)$ and $U_0K(\phi_0)$ for the investigated slurries in their regimes. For both slurries P_y increased and U_0K decreased with increasing ϕ_0. At the same ϕ_0 kaolin slurries have the higher P_y but the lower U_0K than the ball clay slurries. Therefore the kaolin slurries are "stiffer" than the clay slurries. This observation corresponds to the greater β values for the clay slurries in Table 1 when compared with the kaolin slurries. This plastic characteristic apparently degrades in the subsequent settling stage. The dy/dt versus $1/(y - L_c)$ data deviate from the linear regime at $t > 1000$ s.

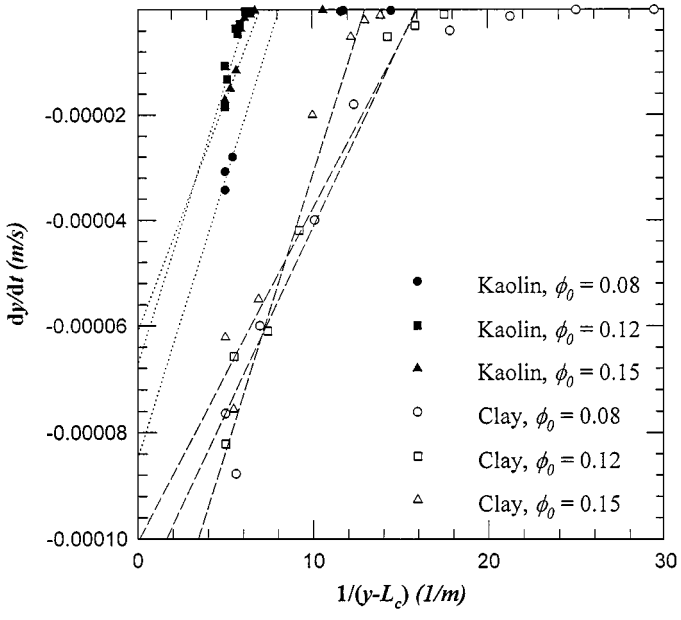

FIG. 8. Plot of dy/dt vs $1/(y - L_c)$ of the slurries with ϕ_0 higher than ϕ_g.

CONCLUSIONS

This study utilized a CATSCAN to measure the spatio-temporal distributions of solids fraction for kaolin and clay slurries at various initial solid concentrations, ϕ_0s. The CATSCAN could not directly measure the null-stress solids fraction (ϕ_g) for the investigated slurries, whose values are estimated using an averaging technique to all around 0.07–0.08, regardless of the ϕ_0.

The experimental range of ϕ_0 (0.01–0.15) has covered both the $\phi_0 < \phi_g$ and $\phi_0 > \phi_g$ cases. The basic settling characteristics are similar for slurries with $\phi_0 > \phi_g$ and vice versa. A constant-ϕ_0 regime is noted for both cases, beneath which a sediment

layer forms. There existed a finite yield stress of the settling sediment indicating that the investigated sediments are plastic fluids. However, the final sediment equilibrated with gravity exhibited no constant-ϕ_0 regime, which indicated purely elastic sediment. The network structure in the slurries degrades gradually in the settling process.

The model parameters of the theory by Buscall and White were regressed from the consolidating sediment data, while those by Tiller and Leu were obtained using the final sediment data. Both results indicate that the clay slurries are more compressible than the kaolin slurries. The higher initial solids fraction would also yield a "stiffer" sediment.

ACKNOWLEDGMENTS

The authors acknowledge support for this work from National Science Council, ROC. The assistance from Prof. F. M. Tiller and Dr. Wenping Li of University of Houston to CATSCAN experiments is highly appreciated.

REFERENCES

1. Coe, H. S., and Clevenger, G. H., *Trans. Am. Inst. Min. Eng.* **55,** 356 (1916).
2. Kynch, G. J., *Trans. Faraday Soc.* **44,** 166 (1952).
3. Talmadge, W. P., and Fitch, E. B., *Ind. Eng. Chem.* **47,** 38 (1955).
4. Tiller, F. M., *AIChE J.* **27,** 823 (1981).
5. Fitch, B., *AIChE J.* **29,** 940 (1983).
6. Font, R., *AIChE J.* **34,** 229 (1988).
7. Font, R., *Chem. Eng. Sci.* **46,** 2473 (1991).
8. Koenders, M. A., and Wakeman, R. J., *Chem. Eng. Sci.* **51,** 3897 (1996).
9. Landman, K. A., Buscall, R., and White, L. R., *AIChE J.* **34,** 239 (1988).
10. Tiller, F. M., and Leu, W. F., *J. Chin. Inst. Chem. Eng.* **11,** 61 (1980).
11. Lee, D. J., and Wang, C. H., *Water Res.* **34,** 1 (2000).
12. Kos, P., *Chem. Eng. Prog.* **73,** 99 (1997).
13. Shirato, M., Murase, T., Tokunaga, A., and Yamada, O., *J. Chem. Eng. Jpn.* **7,** 229 (1974).
14. Tien, C., Bai, R., and Ramarao, B. V., *AIChE J.* **43,** 33 (1997).
15. Buscall, R., and White, L. R., *J. Chem. Soc., Faraday Trans.* **83,** 873 (1987).
16. Auzerais, F. M., Jackson, R., and Russel, W. B., *J. Fluid Mech.* **195,** 437 (1988).
17. Auzerais, F. M., Jackson, R., Russel, W. B., and Murphy, W. F., *J. Fluid Mech.* **221,** 613 (1990).
18. Bergstrom, L., *J. Chem Soc., Faraday Trans.* **88,** 3201 (1992).
19. Shen, C., Russel, W. B., and Auzerais, F. M., *AIChE J.* **40,** 1876 (1994).
20. Johnson, S. B., Scales, P. J., Dixon, D. R., and Pascoe, M., *Water Res.* **34,** 288 (2000).
21. Aziz, A. A. A., de Kretser, R. G., Dixon, D. R., and Scales, P. J., *Water Sci. Technol.* **41,** 9 (2000).
22. Tiller, F. M., and Khatib, Z., *J. Colloid Interface Sci.* **100,** 55 (1984).
23. Lu, W. M., Huang, Y. P., and Hwang, K. J., *Sep. Purif. Technol.* **13,** 9 (1998).
24. Shin, B. S., and Dick, R. I., *J. Environ. Eng. ASCE* **106,** 505 (1980).
25. La Heij, E. J., Kerkhof, P. J. A. M., Kopinga, K., and Pel, K., *AIChE J.* **42,** 953 (1996).
26. Chang, D., Lee, T., Jang, Y., Kim, M., and Lee, S., *Powder Technol.* **92,** 81 (1997).
27. Friedmann, T., and Windhab, E. J., *Sep. Sci. Technol.* **33,** 2221 (1998).
28. Bierck, B. R., Wells, S. A., and Dick, R. I., *J. Water Pollut. Control Fed.* **60,** 645 (1988).
29. David, K. E., Russel, W. B., and Glantschnig, W. J., *Science* **245,** 507 (1989).
30. Bierck, B. R., and Dick, R. I., *Water Sci. Technol.* **22,** 125 (1990).
31. Bierck, B. R., and Dick, R. I., *J. Environ. Eng. ASCE* **116,** 663 (1990).
32. Tiller, F. M., and Yeh, C. S., *Sep. Filtr.* **27,** 123 (1990).
33. Tiller, F. M., Hsung, N. B., and Cong, D. Z., *AIChE J.* **41,** 1153 (1995).
34. Buscall, R., *Colloids Surf.* **43,** 33 (1990).
35. Hounsfield, G. N., British Patent 1,283,915, London, UK (1972).
36. Michaels, A. A., and Bolger, J. C., *Ind. Eng. Chem. Fundam.* **1,** 24 (1962).
37. David, K. E., and Russel, W. B., *Phys. Fluids A* **1,** 82 (1989).
38. Landman, K. A., and Rusel, W. B., *Phys. Fluids A* **5,** 550 (1993).